International Journal of Trend in Research and Development, Volume 13(1), ISSN: 2394-9333
www.ijtrd.com

Temperature Field Analysis of Permanent Magnet-Convex Iron Composite Pole Linear Motor

[1]Shu Li, [2]Yongli Lei, [3]Jianhao Kang, [4]Yushuai Ren and [5]Cong Gao,
[1,2]Zhongshan Inspection Branch for Guangdong Institute of Special Equipment Inspection and Research, Zhongshan, China
[3,4,5]School of Electrical Engineering and Automation, Henan Polytechnic University, Jiaozuo, China

Abstract: The secondary of the permanent magnet-salient iron composite pole linear synchronous motor (PM-SICPLSM) employs a U-type segmented permanent magnet structure, characterized by high magnetic flux focusing capability, low leakage flux, and high thrust density. As the temperature field distribution significantly impacts the operational reliability of the motor, a comprehensive thermal analysis is conducted. First, the structural operating principle of the PM-SICPLSM is examined, and the implications of temperature rise are discussed. Subsequently, the heat source distribution is identified, and key thermal parameters—including losses, thermal conductivity, and heat dissipation coefficients of the components—are calculated. A finite element model (FEM) of the PM-SICPLSM is then established to compute the heat source density and analyze the transient temperature rise of the motor components. This study provides a valuable reference for the thermal design of this motor topology.

Keywords: *Linear Synchronous Motor; Composite Pole Permanent Magnet; Temperature Field Calculation; Finite Element*

I. INTRODUCTION

Permanent magnet synchronous linear motors (PMSLMs) are characterized by high thrust density and high efficiency. Consequently, they are widely utilized in applications such as ropeless hoisting systems, active suspension systems, and machine tools[1]. Driven by the critical demand for high thrust and reduced permanent magnet (PM) costs in PMSLMs, research focused on enhancing thrust density and improving PM utilization has garnered significant attention globally[2]. Reference[3] proposed an 8-pole/9-slot U-shaped permanent magnet synchronous motor. The PM arrangement in this topology consists of a combination of three permanent magnets. Furthermore, a magnetic flux barrier on the quadrature axis ensures that the $q-axis$ inductance is lower than the $d-axis$ inductance.

During the electromechanical energy conversion process, inevitable energy losses are dissipated as heat. Since the windings and silicon steel laminations are concentrated in the primary side, the compact structure leads to localized heat accumulation and a significant temperature rise. Excessive temperature rise can compromise the normal operation and output performance of the equipment. For instance, elevated temperatures accelerate the aging of insulation materials, potentially leading to dielectric breakdown and subsequent system failures. Therefore, it is essential to analyze the temperature rise of each component in the PM-SICPLSM during normal operation to provide a reference for the optimal design of this topology.

A. Structure of PM-SICPLSM

The structure of the PM-SICPLSM is illustrated in Fig. 1. The primary side comprises an iron core and windings, where concentrated windings are employed to effectively mitigate thrust ripple. The secondary side consists of a U-shaped permanent magnet (PM) array, salient poles, and a secondary core. Specifically, the PM arrangement includes two horizontally magnetized rectangular PMs, one vertically upward magnetized rectangular PM, and two sector-shaped PMs with radial magnetization directed toward their curvature centers. To ensure mechanical stability, screw holes are provided at the bottom of the secondary core and salient poles. Furthermore, non-magnetic end-plates are installed at both the front and rear ends to enhance structural integrity.

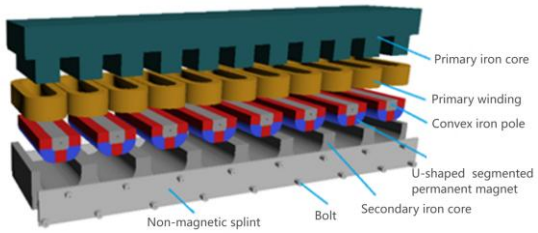

Fig.1 PM-SICPLSM structure diagram

The magnetic flux path illustrated in Fig. 2 originates from the permanent magnet pole and passes sequentially through the salient pole, air gap, primary teeth, primary yoke, and returns through the primary teeth and air gap to the secondary core, forming the main magnetic flux loop. It is evident that the PM-SICPLSM exhibits a favorable magnetic field distribution and a pronounced magnetic flux concentration effect. Compared with a conventional V-type interior permanent magnet synchronous motor (IPMSM) lacking a magnetic bridge, the U-shaped PM arrangement embedded in the secondary effectively minimizes magnetic flux leakage.

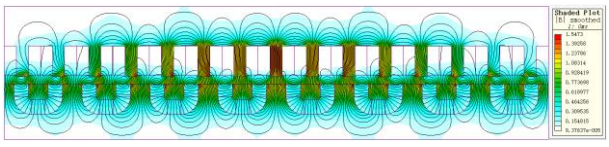

Fig.2 Magnetic field distribution

II. PM-SIICPLSM THREE-DIMENSIONAL GLOBAL TEMPERATURE FIELD ANALYSIS

A. Equivalence of heat source

Bidirectional electromechanical energy conversion occurs within the motor air gap. However, this conversion is not

perfectly efficient; inevitable energy losses are dissipated as heat, leading to a temperature rise during normal operation. As the operation duration increases, the continuous generation of heat exacerbates this temperature rise. Consequently, investigating the thermal characteristics of the PM-SICPLSM is a critical aspect of the design process. It is necessary to quantify the conversion of losses into heat, calculate the heat source density of each component, and analyze the transient temperature rise of the PM-SICPLSM. For the motor investigated in this paper, the primary heat sources include the core losses in the iron components and the copper losses in the windings.

The primary winding of the PM-SICPLSM is housed within the primary slots. Although the winding consists of various materials, the dominant loss source is the resistive heat generated by the current flowing through the copper conductors. For three-phase windings, the copper loss is expressed as:

$$P_{Cu} = 3I_N^2 R \tag{1}$$

where I_N denotes the RMS phase current under steady-state operation, and R represents the winding resistance.

The heat source density of the armature winding is given by:

$$H_{Coil} = \frac{P_{Cu}}{V_{Coil}} \tag{2}$$

where V_{Coil} represents the equivalent volume of the motor winding.

The core loss of the motor is expressed as:

$$P_{Fe} = \sigma_a (fB)^{1.5} + \sigma_e (fB)^2 + \sigma_h fB^h \tag{3}$$

where σ_a、σ_e、σ_h denote the coefficients corresponding to additional loss, eddy-current loss, and hysteresis loss, respectively; f represents the frequency; and B is the magnetic flux density.

Given that analytical iron loss calculations rely on numerous empirical coefficients, finite element analysis (FEA) is employed in this study to accurately determine the core loss of the PM-SICPLSM. Based on these results, the heat source density of the primary iron core is calculated as:

$$H_{Fe} = \frac{P_{Fe}}{V_{Fe}} \tag{4}$$

where VFe denotes the total volume comprising the primary core, secondary core, and salient pole sections.

The heat source density of the permanent magnets is given by:

$$H_{Pm} = \frac{P_{Pm}}{V_{Pm}} \tag{5}$$

where V_{PM} denotes the volume of the permanent magnets, calculated as the product of the magnet cross-sectional area and the axial length of the motor.

The key parameters of the PM-SICPLSM components are listed in Table 1.

Table 1 PM-SICPLSM-related parameters of each component

Unit	Material	Volume (m^3)	locomotor heat source (W/m^3)
The primary iron core	M470-50A	8.232×10^{-4}	4751.46
Secondary core	50W470	5.885×10^{-4}	44794.00
Salient iron pole		9.034×10^{-6}	136768.54
Permanent magnet A	Permanent magnet	5.36×10^{-6}	5539.40
Permanent magnet B		7.05×10^{-6}	780.50
Permanent magnet C		5.98×10^{-6}	741.34
Permanent magnet D		7.05×10^{-6}	871.45
Permanent magnet E		5.36×10^{-6}	6046.19
A-phase winding B-phase winding C -phase winding	Copper	4.69×10^{-5}	702100.47

B. Heat dissipation coefficient calculation

Heat transfer capability is a critical factor influencing the operation and temperature rise of the motor. Convective heat transfer is driven by fluid motion within the motor and involves complex thermal interactions at the motor boundaries. The surface heat dissipation coefficient is influenced by multiple factors, including the surface temperatures of the primary and secondary sections, the ambient air temperature near the structural interfaces, fluid velocity, and the motor's operating conditions. Given the diverse convective heat transfer phenomena present in the proposed motor, the selection of heat dissipation coefficients varies by region. Consequently, this study focuses primarily on the coefficients for the primary outer surface, the secondary outer surface, and the air gap surfaces.

(1) Heat Dissipation Coefficients of Primary and Secondary Outer Surfaces.

The primary outer surface is directly exposed to ambient air. When ambient air serves as the cooling medium, other thermal effects on the motor surface are neglected. It is assumed that the heat dissipation coefficient of the primary surface depends solely on the airflow rate. Consequently, the heat dissipation coefficient of the primary outer surface is calculated as: $\alpha = \alpha_0(1 + k * \sqrt{v})$ (6)

where α_0 represents the heat transfer coefficient of the primary outer surface in still air, typically set to [value]; k denotes a correction factor, generally set to 1.3; and v is the relative air velocity with respect to the motor, corresponding to the primary velocity.

In engineering calculations, the heat dissipation coefficient of the primary outer surface is typically determined

using an empirical formula, expressed as:

$$\alpha_{per} = 40W / m^2 \cdot K \quad (7)$$

The secondary is stationary; thus, the relative air velocity at its outer surface is zero. Consequently, the heat dissipation coefficient of the secondary outer surface is expressed as:

$$\alpha_{sec} = 14.2W / m^2 \cdot K \quad (8)$$

(2) Heat Dissipation Coefficients of Primary and Secondary Surfaces in the Air Gap

During motor operation, the movement of the primary influences the air within the air gap, while the secondary surface impedes the airflow. Consequently, the heat dissipation coefficients for the primary and secondary surfaces in the air gap are expressed as follows:

$$\alpha = k_\delta \left[1 + \left(\frac{v_\delta}{2} \right)^{\frac{1}{2}} \right] \quad (9)$$

Where k_δ denotes the velocity of the PM-SICPLSM, and v_δ is empirically set to 28.

Discrepancies exist between the three-dimensional and two-dimensional temperature field results of the motor. Therefore, an equivalent transformation is performed using Eq. (10).

$$\alpha_1 S_1 = \alpha_2 S_2 \quad (10)$$

where α_1 and S_1 represent the surface heat dissipation coefficient and the secondary outer surface area in the three-dimensional temperature field, respectively; α_2 and S_2 denote the corresponding surface heat dissipation coefficient and secondary surface area in the two-dimensional temperature field.

C. Calculation of thermal conductivity

The motor comprises various materials, including metals and insulators. Thermal conductivity varies among these materials and is predominantly influenced by temperature. Provided the temperature remains below the melting or vaporization point, the thermal conductivity of most substances is assumed to vary linearly with temperature. Consequently, it is expressed as:

$$\lambda = \lambda_0 (1 + bt) \quad (11)$$

where λ_0 represents the thermal conductivity at 0°C, and b denotes the experimentally determined temperature coefficient of the material.

The silicon steel laminations used in the motor typically have a thickness of 0.35 mm or 0.5 mm. The stacking factor is inversely proportional to the interlaminar air gap and proportional to the effective thermal conductivity. In this paper, the thermal conductivity in the plane of the laminations is 42.5 $W/m^2 \cdot K$, while the thermal conductivity normal to the laminations is taken as 1.19 $W/m^2 \cdot K$.

The motor consists of diverse materials, including silicon steel laminations, enameled wire, magnetic media, and epoxy resin. Consequently, thermal conductivity varies significantly across different components. The thermal conductivities of the primary materials are listed in Table 2.

Table 2: Thermal conductivity of different materials

Materials	Thermal conductivity (λ/W.m.K)	Materials	Thermal conductivity (λ/W.m.K)
Class A insulation winding	0.4-0.6	Mica	0.4-0.6
Class B insulation winding	0.12-0.16	Dry impregnated paint	0.14-0.16
Class C insulation winding	About 0.26	Oil	0.12-0.17
Oil-immersed electrical paperboard	0.25	Stationary air	0.025
Paint-impregnated electrical paperboard	0.14	Timber	0.14-0.3
Adhesive cardboard	0.23-0.28	Epoxy resin	0.2-0.5

3 Temperature field simulation analysis

To simplify the computation while maintaining accuracy, the following assumptions are made for the motor thermal field analysis:

1. The ambient temperature remains constant.
2. Temperature gradients within individual components of the same material are neglected.
3. Heat sources within each motor component are uniformly distributed, and the thermal impact of mechanical losses is neglected.
4. Composite regions are treated as homogenized domains, using equivalent thermal conductivity.

Based on these assumptions and the preceding analysis, the temperature field model of the motor is established, as shown in Fig. 3.

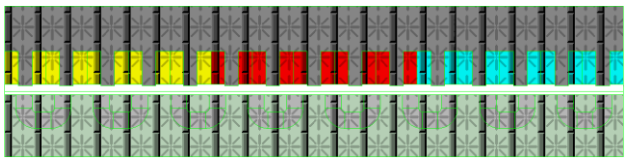

Fig.3 Temperature field section of PM-SICPLSM

The temperature distribution of the PM-SICPLSM, obtained via the finite element model, is presented in Fig. 4. It is evident that the primary temperature significantly exceeds that of the secondary. Furthermore, a distinct temperature gradient is observed within the primary, characterized by higher temperatures in the central region and lower temperatures at both ends. This phenomenon is attributed to two factors: first, the heat generated by the primary winding is substantially larger than that of the secondary; second, the central region experiences poorer heat dissipation conditions due to limited air exposure compared to the ends.

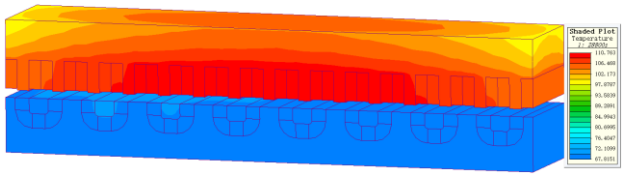

(a) The overall temperature distribution of the motor

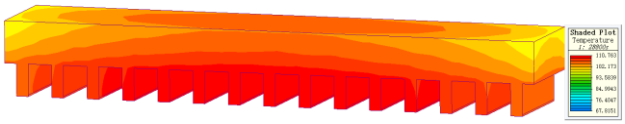

(b) Primary core

(c) Primary winding

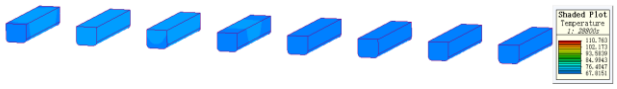

(d) Convex iron

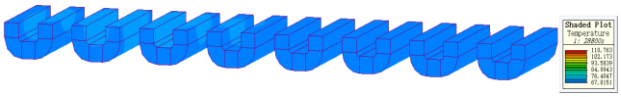

(e) U-type permanent magnet

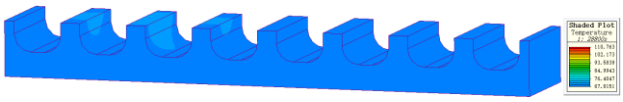

(f) Secondary core

Fig.4 PM-SICPLSM 3D temperature field distribution

Fig. 5 illustrates the temperature rise of different primary teeth in the PM-SICPLSM finite element model at a constant speed. The results indicate that the temperature of the primary core adjacent to the windings increases significantly, as the heat generated by winding losses is the dominant thermal source. Due to the open structure of the primary ends, the lowest temperature of the primary core is observed at the four corners of the primary yoke. In the steady state, the temperatures at specific locations on the teeth reach 110.7 °C, 70.3 °C, and 70.2 °C, respectively. These observations substantiate the phenomenon that the primary side temperature is higher than that of the secondary side.

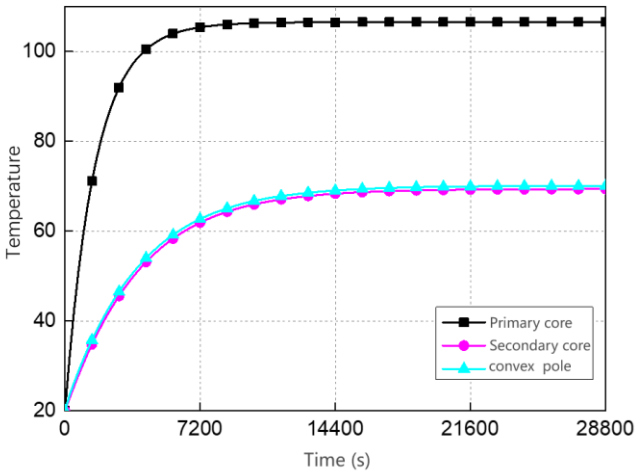

Fig.5 The temperature rise of the primary core, Convex iron and secondary core

The U-shaped permanent magnet structure of the PM-SICPLSM consists of five distinct permanent magnets (PMs). Since excessive temperature rise may induce irreversible demagnetization, analyzing the thermal behavior of individual PMs is essential for the comprehensive thermal analysis of the machine. These five magnets are designated as: rectangular magnet A, sector magnet B, rectangular magnet C, sector magnet D, and rectangular magnet E. Fig. 6 illustrates the temperature rise of these magnets at a constant speed. The thermal trends across the five PMs are similar. Notably, magnets D and E, located near the motor center, exhibit slightly higher temperatures than the others. Due to superior natural heat dissipation at the motor ends, magnets A and B maintain lower temperatures; specifically, the temperature of magnet A is slightly higher than that of magnet B.

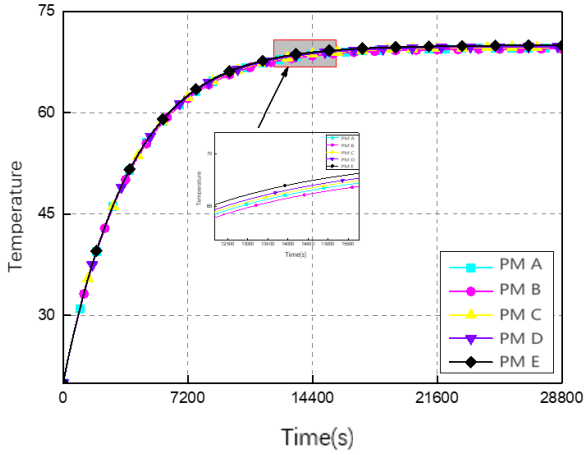

Fig. 6 The temperature rise of 5 permanent magnets in PM-SICPLSM

Motor heating is primarily attributed to winding losses, core losses, and permanent magnet eddy current losses. Among these, winding loss constitutes the dominant heat source. Excessive winding temperatures pose a risk of coil insulation failure, thereby jeopardizing the reliable operation of the motor. Consequently, analyzing the transient temperature rise of the three-phase windings is essential. Fig. 7 illustrates the temperature rise of the PM-SICPLSM windings at a constant speed. As observed, the temperature profile of the Phase A winding is slightly lower than that of Phases B and C.

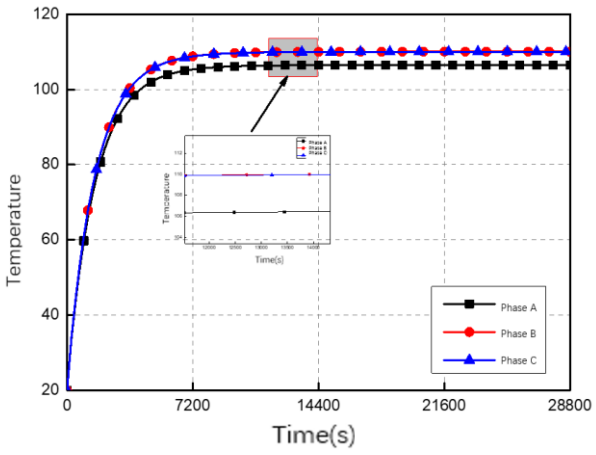

Fig.7 Temperature rise of three-phase windings at the same speed

CONCLUSION

In this paper, the motor heat sources are analyzed, and key thermal parameters—including equivalent thermal conductivity, air gap effective thermal conductivity, and surface heat dissipation coefficients—are calculated. A finite element model of the motor is established, and the thermal performance is evaluated based on temperature rise simulation results. Calculations indicate that during steady-state operation, the windings constitute the dominant heat source, resulting in heat accumulation primarily concentrated in the motor primary. Due to the open structure of the PM-SICPLSM, significant end effects are observed; specifically, the primary ends benefit from superior heat dissipation conditions, facilitating rapid heat rejection. Consequently, the peak temperature rise occurs in the central region of the primary, with a thermal gradient decreasing from the center toward the ends. Meanwhile, the temperature rise of the secondary core remains relatively low, exhibiting a gradual decrease from the central axis toward both sides.

References

[1] Lu Qinfen, Shen Yiming, Ye Yunyue. “Review of structure and research development of permanent magnet linear motor,” *Proceedings of the CSEE*, vol. 39, no. 9, pp. 2575-2588.

[2] Kim S A, Zhu Y W, Lee S G, et al. “Electromagnetic Normal Force Characteristics of a Permanent Magnet Linear Synchronous Motor with Double Primary Side”. *IEEE Transactions on Magnetics*, vol. 50, no. 1, pp. 1204-1207,

[3] H. Tu, X. Zhu, L. Quan, L. Chen and Z. Xiang, "Electromagnetic performances analysis of flux-intensifying permanent magnet synchronous machine with modular fractional slot concentrated windings," *2014 17th International Conference on Electrical Machines and Systems (ICEMS)*, Hangzhou, China, 2014, pp. 1990-1994

[4] Wang Xudong, XIAO Chi, FENG Haichao, “Characteristic analysis and optimization of U-type permanent magnet flux-switching linear motor” *Electric Machines and Control*, vol. 25, no. 2, pp.132-140, Feb 2021.

[5] Liu Zhiyou, Zhou Haibo, Wang Xiaoling, et al. “Design and analysis of micro linear-rotary voice coil motor”. *Transducer and Microsystem Technologies*, vol. 37, no. 7, pp. 97-98 + 102, 2018.

[6] P. S. Shin, S. H. Woo, Y. Zhang and C. S. Koh, "An Application of Latin Hypercube Sampling Strategy for Cogging Torque Reduction of Large-Scale Permanent Magnet Motor," in *IEEE Transactions on Magnetics*, vol. 44, no. 11, pp. 4421-4424, Nov. 2008

[7] X. Xu, Z. Sun, B. Du and L. Ai, "Pole Optimization and Thrust Ripple Suppression of New Halbach Consequent-Pole PMLSM for Ropeless Elevator Propulsion," in *IEEE Access*, vol. 8, pp. 62042-62052, 2020.

Introduction of the author: Lei Yongli (1980-), male, master, research direction: electromechanical system design and control